The Astrophysical Journal Letters, 887:L18 (13pp), 2019 December 10 https://doi.org/10.3847/2041-8213/ab595d

Multispacecraft Observation of Unidirectional and Bidirectional Alfvén Waves within Large-scale Magnetic Clouds

Zehao Wang[1,2], Xueshang Feng[1], and Jianchuan Zheng[3]
[1] SIGMA Weather Group, State Key Laboratory of Space Weather, NSSC, Chinese Academy of Sciences, Beijing 100190, People's Republic of China
zhwang@spaceweather.ac.cn, fengx@spaceweather.ac.cn
[2] College of Earth Sciences, University of Chinese Academy of Sciences, Beijing 100049, People's Republic of China
[3] Shenzhen Astronomical Observatory, Shenzhen National Climate Observatory, Shenzhen 518040, People's Republic of China
Received 2019 July 9; revised 2019 November 18; accepted 2019 November 20; published 2019 December 10

Abstract

Recent years have seen growing evidence of the existence of Alfvén waves within interplanetary magnetic flux ropes, which are believed to be an important aspect of dynamics connecting the Sun and the heliosphere. Previous studies, due to localized observation by single spacecraft, focused on sunward or antisunward Alfvén waves propagating along with magnetic field lines. In this Letter, for the first time, we use multispacecraft observations to verify and analyze two large-scale magnetic clouds (MCs), when the spacecraft had quite different spatial separations. What surprises us is that not only unidirectional but bidirectional Alfvén waves exist in the large-scale MC, which is rooted to the Sun. We speculate that unidirectional Alfvén waves within an MC are generated by distortions produced within a preexisting flux rope, and bidirectional Alfvén waves are emitted from the center of reconnection and then travel outward along with two loop legs of an MC.

Unified Astronomy Thesaurus concepts: Solar coronal mass ejections (310); Solar wind (1873); Alfven waves (23)

1. Introduction

Coronal mass ejection (CME) is known as a large-scale phenomenon involving the violent explosion of massive magnetized plasmas and huge energy from active solar source regions into interplanetary space. Interplanetary coronal mass ejections (ICMEs) are considered to be the interplanetary manifestations of CMEs, and magnetic clouds (MCs), the most familiar flux ropes in the solar wind, form a subset of ICMEs (Gosling 1990). Alfvén waves are recognized as an important aspect of dynamics connecting the Sun and the heliosphere, which can carry significant energy from the lower atmosphere to solar wind. Previous studies have shown that Alfvén waves are seldom capable of surviving in ICMEs (e.g., Belcher & Davis 1971; Liu et al. 2006). However, recent years have seen growing evidence of the constant existence of Alfvén waves in ICME or MC (e.g., Marsch et al. 2009; Yao et al. 2010; Liang et al. 2012). Thus Alfvén waves in ICME have received considerable attention (e.g., Liu et al. 2006; Li et al. 2016).

Generally, Alfvén waves are expected to be present in two forms: arc-polarized Alfvén waves that have been frequently observed in the solar wind (e.g., Belcher & Davis 1971; Barnes & Hollweg 1974; Wang et al. 2012), and tube modes in ideal magnetic flux ropes, such as the torsional mode (e.g., Doorsselaere et al. 2008; Jess et al. 2009; Vasheghani et al. 2011; Shelyag et al. 2013). In the solar atmosphere, magnetic field lines generally clump together to form magnetic flux tubes, thus they provide an ideal medium for tube modes. The proposed generation mechanisms for Alfvén waves in magnetic flux ropes include distortions produced within a preexisting flux rope that erupted from the Sun (Gosling et al. 2010), and magnetic reconnection during the eruption (Copil et al. 2008; He et al. 2018). In addition, Alfvén waves might be produced during the unwrapping process of flux ropes (Longcope & Welsch 2000; Fan 2009).

Torsional Alfvén waves, one of the tube modes, act as azimuthal oscillations of magnetic field and plasma velocity on the magnetic surfaces, with no density perturbations. Gosling et al. (2010) first observed torsional Alfvén waves embedded within a small-scale magnetic flux rope at 1 au. Raghav & Kule (2018) also presented unambiguous evidence of torsional Alfvén waves in the interacting region after the super-elastic collision of multiple CMEs. Furthermore, Guo et al. (2019) obtained a possible detection clue of torsional Alfvén waves that the magnetic field inside MC underwent alternate rotations along an arc through a relatively small angle. Once the magnetic flux rope undergoes eruption, no matter which mode exists in it, we have a high probability to detect Alfvén waves in interplanetary space.

In this Letter, we first report that two large-scale MC events were captured by both *STEREO* A and *WIND* spacecraft which have well separated longitudinal alignment. The observations provide important information that there are unidirectional or bidirectional Alfvén waves embedded within a magnetic flux rope rooted at both ends in the solar photosphere.

2. Data

The *WIND* spacecraft and *Solar and Heliospheric Observatory* (*SOHO*) spacecraft were located around the Lagrangian point L1 upstream of the Earth. For *WIND*, we used the 3 s resolution magnetic data near 1 au from the Magnetic Fields Investigation (Lepping et al. 1995). The plasma and suprathermal electron data are from the 3D Plasma and Energetic Particles Experiment (Lin et al. 1995). The *SOHO*/Large Angle and Spectromeric Coronagraph Experiment (LASCO) carries two working cameras (C2 and C3) photographing images covering the corona from 1.5 Rs to 6 Rs and from 3.7 Rs to 30 Rs, respectively (Brueckner et al. 1995). The twin *STEREO* spacecraft (denoted by *STA* and *STB*) travel in Earth's orbit with an increasing separation to the Earth. The in situ data of interplanetary magnetic field are from in situ measurements of particles and CME transients (Acuña et al. 2008) and plasma and suprathermal ion composition (Galvin et al. 2008)

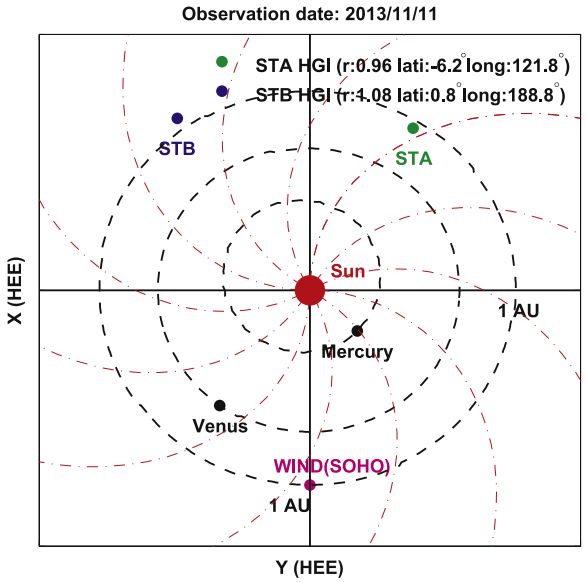

Figure 1. Positions of the spacecraft (*WIND*, *SOHO*, *STEREO* A, and B) and planets in heliocentric Earth–ecliptic (HEE) coordinates on 2013 November 11. The red dotted–dashed curves approximately represent the tracks of solar wind. HGI stands for heliographic inertial coordinates.

instruments. The suprathermal electron pitch angle distribution with 30 s time resolution was obtained by the Solar Wind Electron Analyzer (Sauvaud et al. 2008). COR1 and COR2 on board twin *STEREO* spacecraft monitor the corona and interplanetary space from 1.4 Rs to 4 Rs and from 2.5 Rs to 15 Rs, respectively (Howard et al. 2008). These three imagers (*SOHO*, *STA*, and *STB*) provide multiangle observations of the kinematic evolution of a CME, and the multispacecraft measurements (*WIND*, *STA*, and *STB*) well separated in longitude allow us to infer the spatial and temporal evolution of a CME.

3. Observations and Analysis

3.1. CME1/MC1: 2013 November 7 00:00:06

Figure 1 displays the positions of four widely separated spacecraft (*WIND*, *SOHO*, *STA*, and *STB*) in heliocentric Earth–ecliptic (HEE) coordinates on 2013 November 11. The HEE coordinates are fixed with respect to the Earth–Sun line, where the *X*-axis is from the Sun toward the Earth, and the *Z*-axis is perpendicular to the plane of the Earth's orbit around the Sun, with the *Y*-axis completing the right-handed triad. *STA* and *STB* were 148.°9 west and 143.°9 east of the Earth with a distance of 0.96 au and 1.08 au from the Sun, respectively.

SOHO/LASCO C2 camera captured a westward CME (denoted as CME1) starting at 00:00:06 UT on 2013 November 7, whose source location is S11W97 retrieved from the *SOHO* LASCO CME CATALOG (https://cdaw.gsfc.nasa.gov/CME_list/halo/halo.html). As shown in Figure 2, CME1 quickly developed into the FOVs of all three coronagraphs in a halo shape. In the views of *STA* and *STB*, the CME1 presented a halo shape with the main part expanding toward the east. Considering the positions of three spacecraft, it is suggested that the initial CME1 direction of propagation is located between the Sun–*SOHO* line and the Sun–*STA* line. Obviously, it traveled in the ecliptic plane. Based on the triangulation method (Jang et al. 2016), we determine that CME1's angular width is approximately 152°, slightly greater than 148.°9. It is worth noting that CME1 is expanding during propagating away from the Sun (for instance, CME1's angular width is ∼133° in Figure 2(b1)). This means that CME1's angular width will be much greater than the separation angle between *WIND* and *STA* when it arrives at 1 au. Thus it is reasonably conjectured that CME1 will sweep *WIND* and *STA* with its two flanks respectively. To verify this, we check in situ measurements from these two spacecraft.

Generally, the travel time of CME is about 2–5 days (e.g., Gopalswamy et al. 2001; Shi et al. 2015), thus we examine the in situ data from *WIND* and *STA* for 6 days starting from 2013 November 7. For *WIND* observation, only one interplanetary CME has been identified (denoted as MC1_WIND, see the shadow region in Figure 3) in this interval. MC1's encounter began at 17:42 UT on 2013 November 11, and ended at 02:01 UT on 2013 November 12. All the MC signatures are very clear, which basically include (1) the enhanced magnetic field strength, (2) large and smooth rotation of magnetic field direction, (3) declining profile of solar wind velocity, (4) bidirectional suprathermal electron strahls, (5) low proton temperature, and (6) low proton $\beta(\leqslant 0.1)$ (e.g., Burlaga et al. 1981). The calculated average speed of MC1_WIND is about 482 km s^{-1}, which can come to a conclusion that the explosion time of the corresponding CME is around the beginning of 2013 November 8 (Möstl et al. 2014). After checking the coronal images within 2 days before and after, we confirm no other CMEs except CME1 toward *WIND*. It is conclusive that MC1_WIND is the interplanetary counterpart of CME1.

Then only one interplanetary MC structure is identified by *STA* (denoted as MC1_STA in Figure 4), which satisfies all the previously mentioned six signatures of a typical MC. Its front boundary is at about 06:13 UT on 2013 November 12 and the rear boundary is at about 00:00 UT on the next day. Furthermore, a shock of MC was detected at about 10:31 UT on 2013 November 11. The average speed of solar wind during the MC1_STA is about 370 km s^{-1}, suggesting the corresponding CME lifting off from the Sun around 00:00 UT on 2013 November 8. During the interval of 2 days before and after this timepoint, three coronagraphs capture only CME1 directing to *STA*. Therefore, we verify that MC1_WIND and MC1_STA are both the observational evidences of CME1 at 1 au.

After scrutinizing the configurations of MC1_WIND and MC1_STA, many similarities are identified: (1) low density, low proton temperature, and low proton β, (2) bidirectional suprathermal electron strahls, (3) equal magnetic field strength (∼7.5 nT), (4) constant magnetic field azimuthal angle, and (5) magnetic field elevation angles change from positive to negative, of which the scales are 40° ∼ 20° and 45° ∼ −45°. Beyond that, it is surprised that there is a high correlation between the velocity and the magnetic field components in both MC1_WIND and MC1_STA. In order to further confirm the nature of the fluctuations, we conduct a Walén test (Sonnerup et al. 1987) and the correlation analysis (Denskat & Burlaga 1977; Tian et al. 2010).

To examine the Walén relation, a good deHoffman–Teller (HT) frame needs to be found. Hence, we divide MC interval into multiple segments with a duration varying from 20 minutes to 2 hr to avoid the expanding effect of MC during the propagating process. The averaged convection electric field ($E_{\rm HT} = -V_{\rm HT} \times B$) in each segment can be minimal but cannot be vanished. The strong correlation between components of

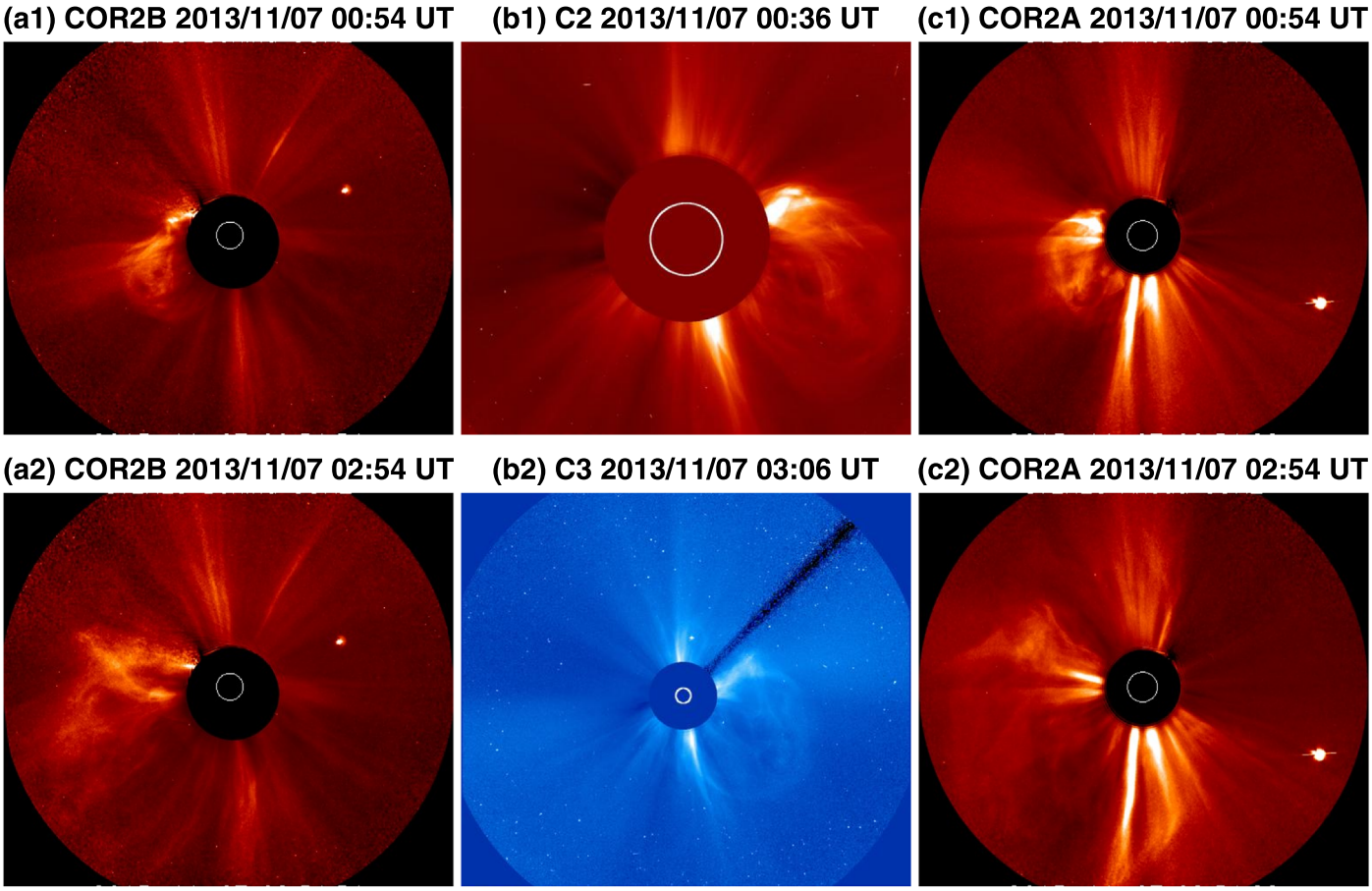

Figure 2. Snapshots of the CME taken by (a) *STB*/COR, (b) *SOHO*/LASCO, and (c) *STA*/COR on 2013 November 7.

$V_{\rm rtn}$ − $V_{\rm HT}$ and the Alfvén velocity ($V_{\rm A}=\frac{\delta B}{\sqrt{\mu_0 m N_p}}$, where m, N_p, and μ_0 refer to proton mass, proton number density, and permeability of free space) confirms the presence of Alfvén waves (Gosling et al. 2010; Guo et al. 2019). Denskat & Burlaga (1977) and Tian et al. (2010) suggested that Alfvénic fluctuations could be determined if two or more correlation coefficients are greater than 0.6 in flux ropes. Figure 5 shows the linear fit and correlation coefficients (in the *r*-, *t*-, and *n*-components) for selected segments from MC1_WIND (left) and MC1_STA (right). The slopes of the linear regression fitting in MC1_WIND are 0.95, 0.73, and 0.7, and the slopes in MC1_STA are 0.89, 0.6, and 0.62. Meanwhile, the observed values of correlation coefficients in both MC1_WIND and in MC1_STA coincide with the criteria mentioned above, meaning that the anti-magnetic-field-direction Alfvén waves are observed by *WIND* and *STA*, respectively. Thus it can be verified that the unidirectional anti-magnetic-field-direction Alfvén waves are embedded within the whole MC1.

3.2. CME2/MC2: 2011 October 22 10:24:05

The positions of *STA* and *STB* in HEE coordinates at the beginning of 2011 October 25 are plotted in Figure 6. At that time, *STA* is separated away from *WIND* by 105°.3 and *STB* by 100°.6. According to the observation of *SOHO*, a halo CME (denoted as CME2) erupted from N25W77 at 10:24:05 UT on 2011 October 22 (see Figure 7). In view of *STA*, CME2 looks like an east limb event, but a west limb event in *SOHO*. It can be roughly identified that the spreading direction of CME2 is between the Sun–*STA* line and the Sun–*SOHO* line. Meanwhile, CME2's angular width is 180° (see Shi et al. 2015). Because it is greater than 105°.3, such a giant CME2 is wide enough to encounter *STA* and *WIND* spacecraft.

Based on the analysis of a 6 day observation of *WIND* after the eruption of CME2, only one MC structure is identified (hereinafter denoted as MC2_WIND). The shock was first encountered by *WIND* at 17:39 UT on 2011 October 24, and the rope was encountered from 00:32 UT to 12:41 UT on 2011 October 25 (see Figure 8). In order to confirm the track of CME2 in the Sun–Earth line, the J-map is used (Davies et al. 2009). Both *STA* and *STB* carry HI1 and HI2 imagers taking pictures of interplanetary space seamlessly. We choose the slice along the ecliptic plane toward *WIND* to construct the J-map, where any stripe with a positive slope represents a featured element propagating away from the Sun. Figure 9 illustrates the J-map of *STB* during 2011 October 22–26 (obtained from https://www.helcats-fp7.eu/catalogs/wp2_cat.html), where the horizontal black line marks the position of the Earth and the red dots represent the trajectory of the leading edge of CME2. We verify that CME2 hits the Earth, and this result is also verified by Shen et al. (2014). Furthermore, Shi et al. (2015) forecasted the arrival time and speed of CME2 with the Graduated Cylindrical Shell and Drag Force Model, which is consistent with in situ arrival time and speed of MC2_WIND.

Similarly, after checking data of *STA* during the same period, a traditionally defined MC can be discerned (denoted as

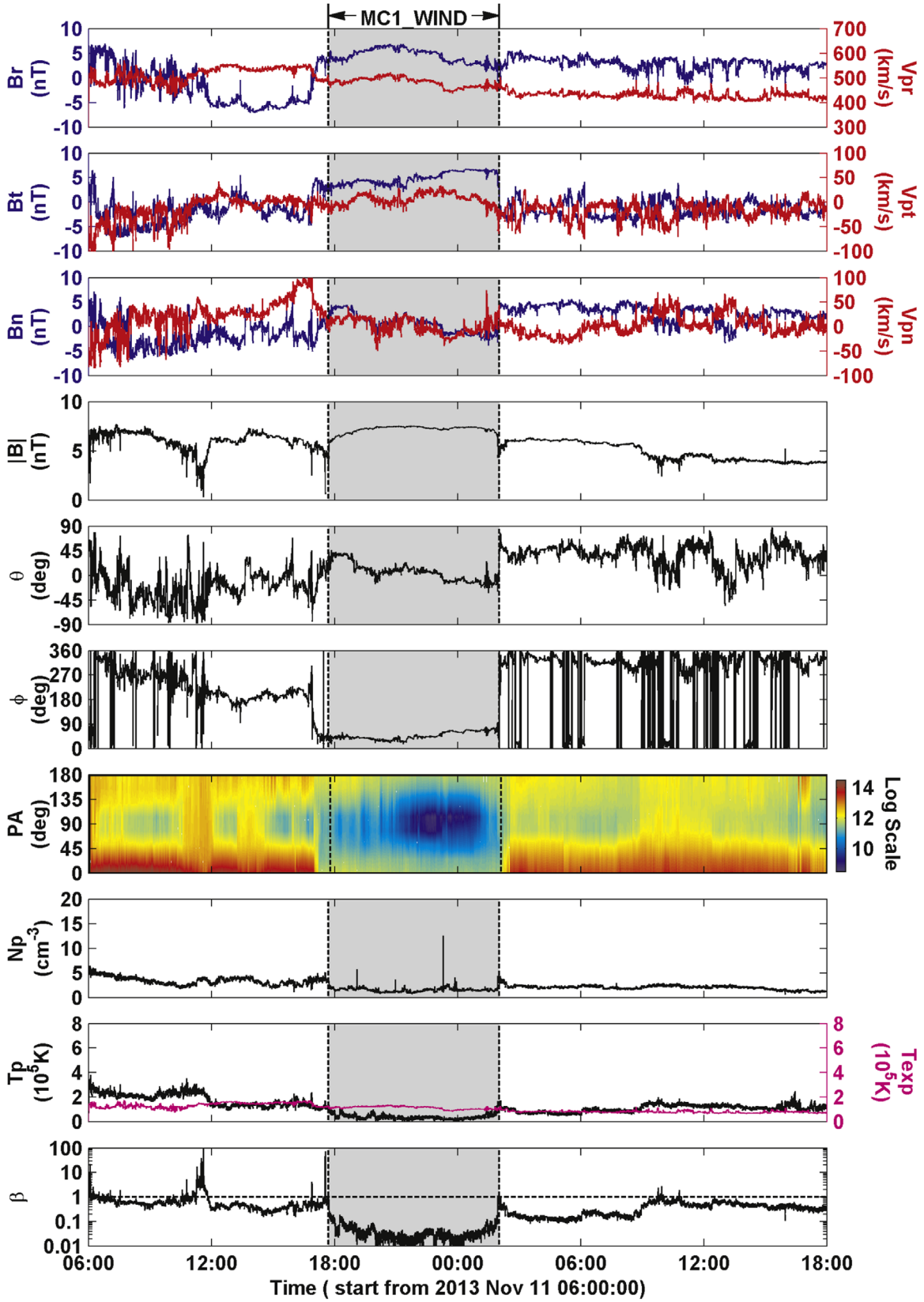

Figure 3. Solar wind parameters observed by *WIND* with a time resolution of 3 s from 06:00 UT on 2013 November 11 to 18:00 UT on 2013 November 12. From top to bottom: magnetic field and proton velocity components in RTN coordinates, magnetic field magnitude (|*B*|), elevation angle (θ) and azimuthal angle (ϕ) of field direction, pitch angle (PA) of suprathermal electron strahls ~300 eV, proton density (N_p), proton temperature (T_p) overlaid with the expected temperature ($T_{\rm exp}$), and proton β.

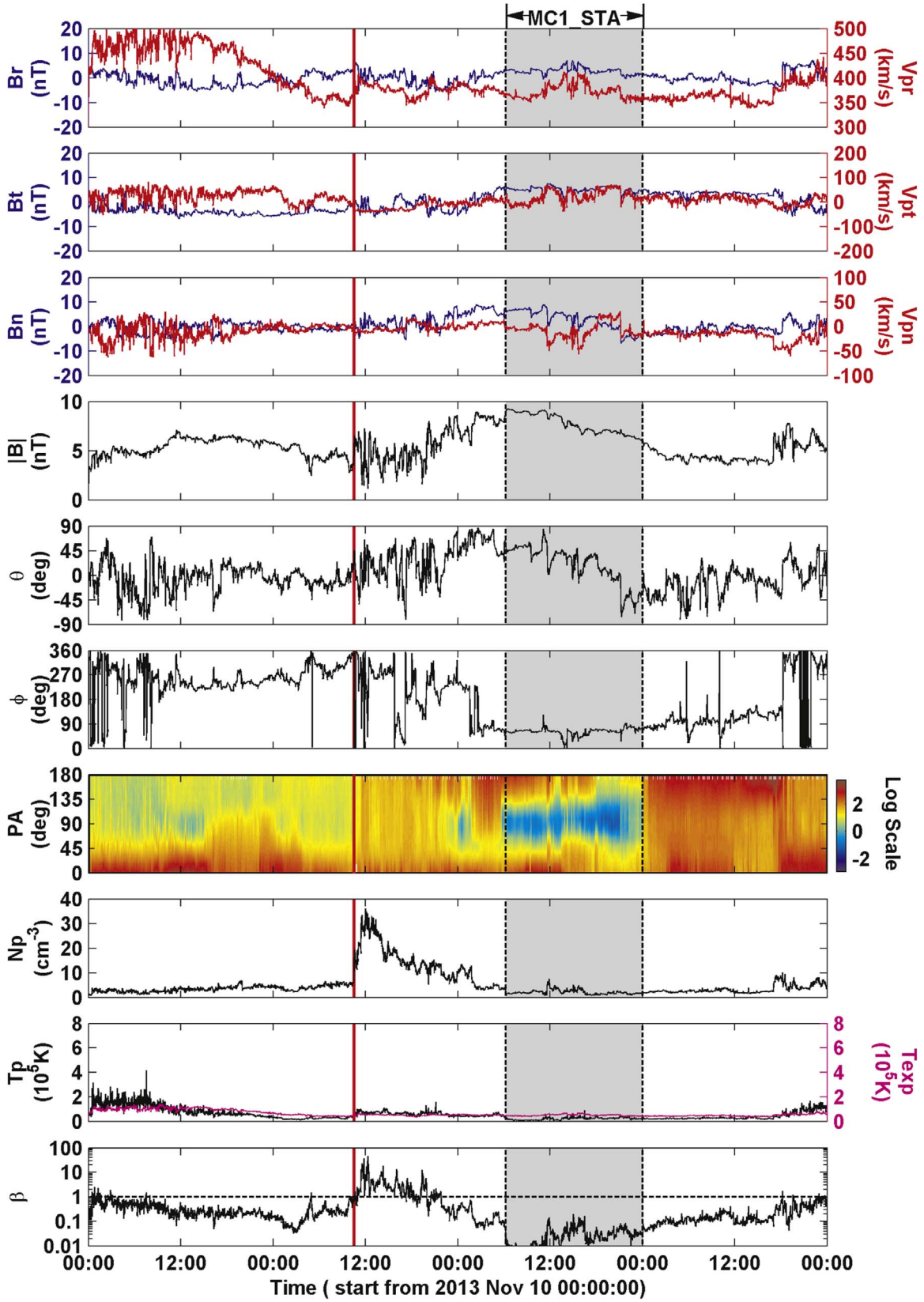

Figure 4. Solar wind parameters observed by *STA* with a time resolution of 1 min during 2013 November 10–14. From top to bottom: magnetic field and proton velocity components in RTN coordinates, magnetic field magnitude ($|B|$), elevation angle (θ) and azimuthal angle (ϕ) of field direction, pitch angle (PA) of suprathermal electron strahls ~246.6eV, proton density (N_p), proton temperature (T_p) overlaid with the expected temperature ($T_{\rm exp}$), and proton β.

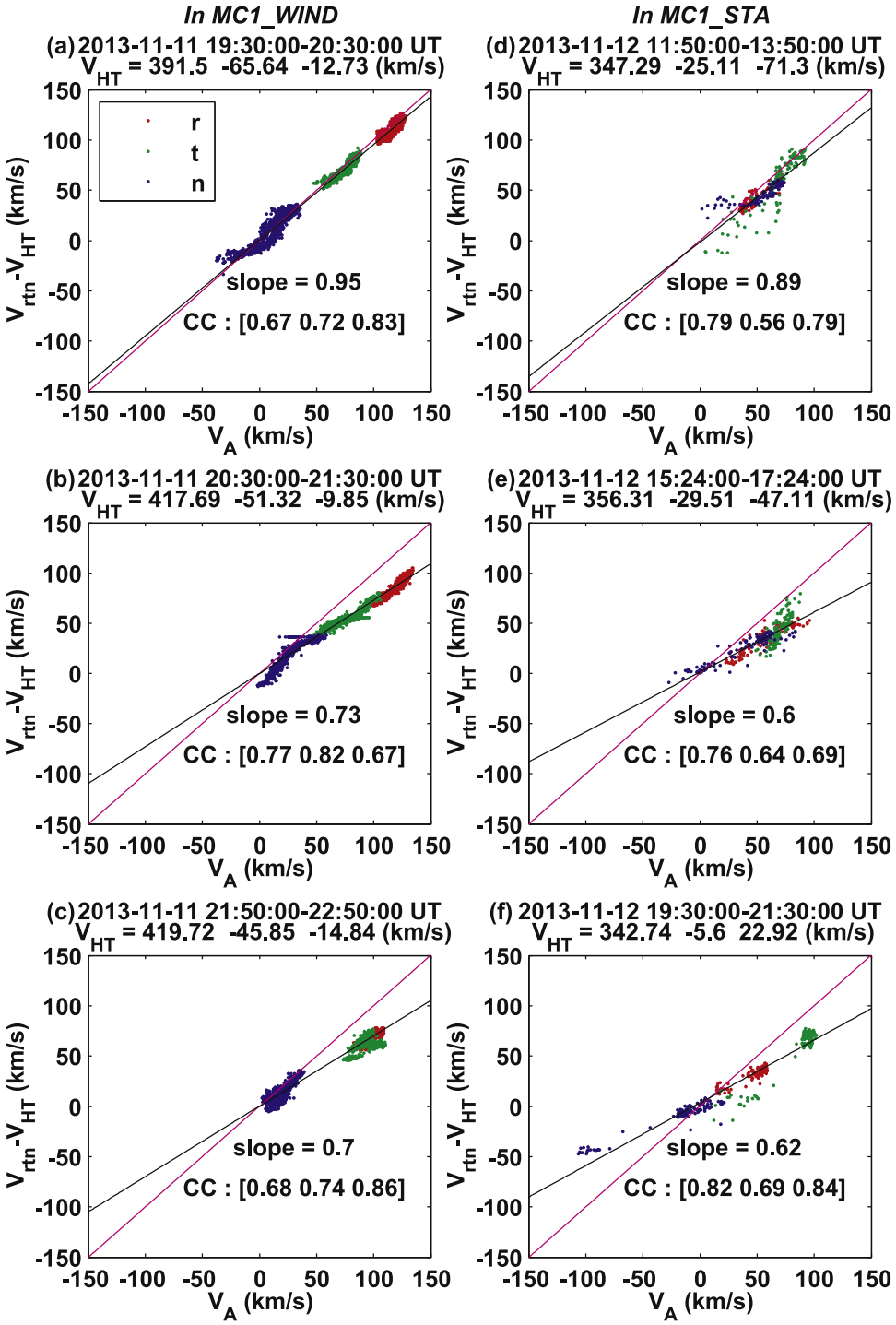

Figure 5. Plasma velocity in the HT frame ($V_{\rm rtn} - V_{\rm HT}$) vs. Alfvén velocity ($V_{\rm A}$) of all three components for each segment. The HT frame velocity, correlation coefficient, and the linear regression fitting slope are shown. Panels (a)–(c) show the analysis results from MC1_WIND, and panels (d)–(f) from MC1_STA.

MC2_STA in Figure 10). MC2_STA started at 15:47 UT on 2011 October 25, ended at 10:25 UT on 2011 October 26. It drove a forward shock, which is indicated by red vertical lines at 04:51 UT on 2011 October 25. The calculated average speed of MC2_STA is about 400 km s^{-1}, which can lead to the conclusion that the explosion time of the corresponding CME is around 12:00 UT on 2011 October 21. After checking the coronal images within 2 days before and after, about nine hours before CME2 there was only one other CME that erupted (denoted as CME*, not shown), of which the source location was N35W40 and the start time at *SOHO* was 01:25:53 UT on 2011 October 22, earlier than CME2. CME* missing the Earth has been verified by Shen et al. (2014). Meanwhile, we identify an MC-like ejecta before MC2_STA (as indicated by dashed lines in Figure 10). The interval of the MC-like ejecta is between 20:50 UT on 2011 October 23 and 10:45 UT on 2011 October 24. It only satisfies four of the above characteristics, including enhanced magnetic field, declined solar wind speed, low temperature, and low proton β except bidirectional suprathermal electron strahls and smooth rotation of magnetic

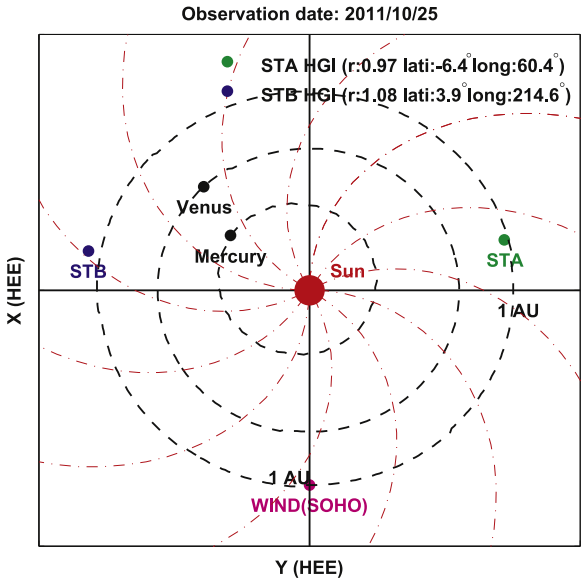

Figure 6. Positions of the spacecraft (*WIND*, *SOHO*, *STEREO* A, and B) and planets in heliocentric Earth–ecliptic (HEE) coordinates on 2011 October 25.

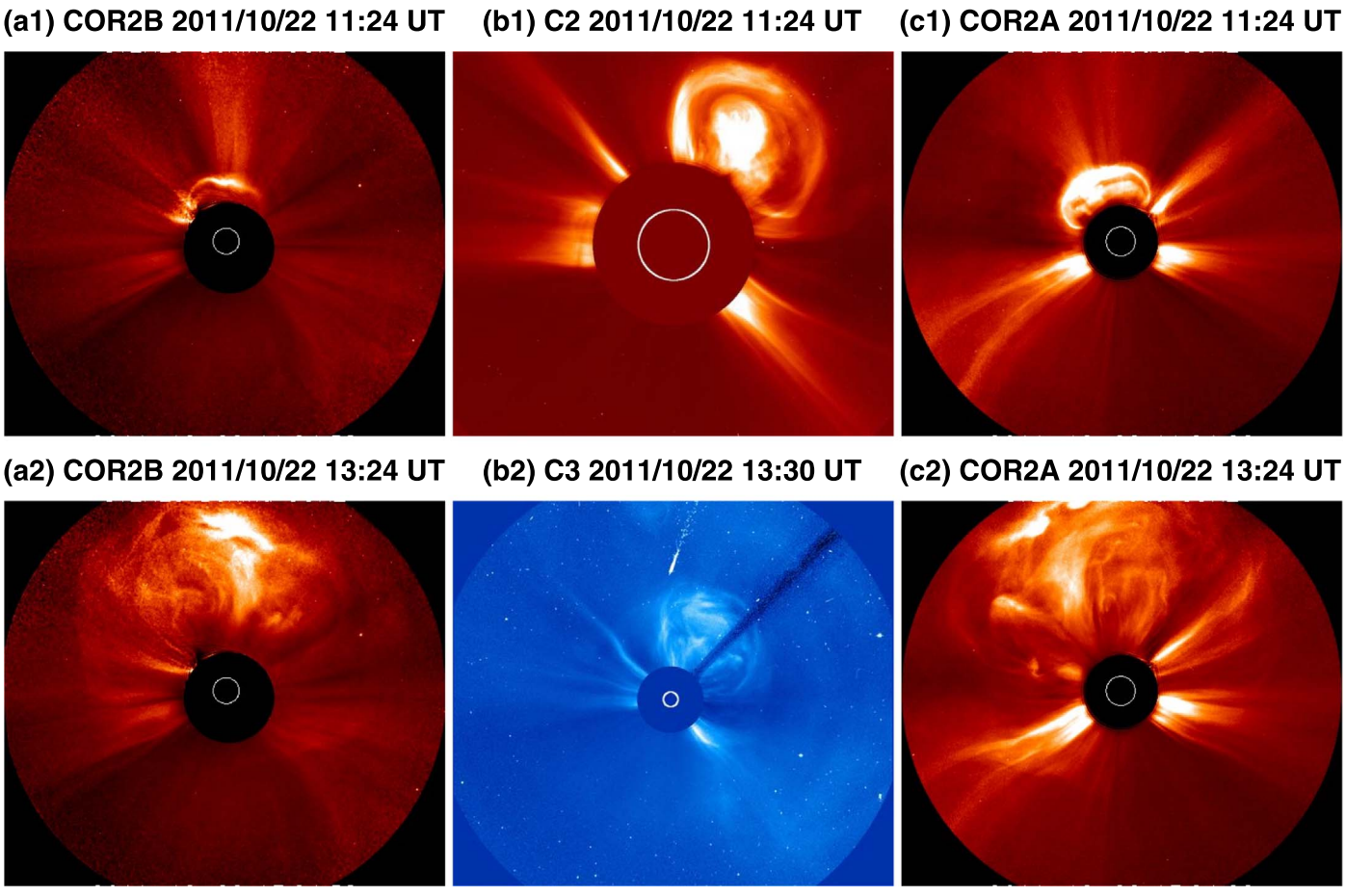

Figure 7. Snapshots of the CME taken by (a) *STB*/COR, (b) *SOHO*/LASCO, and (c) *STA*/COR on 2011 October 22.

field vector. In light of the *SOHO* LASCO CME CATALOG, the measurement position angle (MPA) of CME* is 354°, which is measured counterclockwise from solar north for the CME's fastest segment of the leading edge. Hence, it can come to a conclusion that the initial CME* direction of propagation is approximately perpendicular to the plane of the Earth's orbit around the Sun. This might be the main reason why CME* missed *WIND* and the MC-like structure was observed by *STA* rather than the MC structure. In addition, we use the Drag-based Model (http://oh.geof.unizg.hr/DBM/dbm.php)

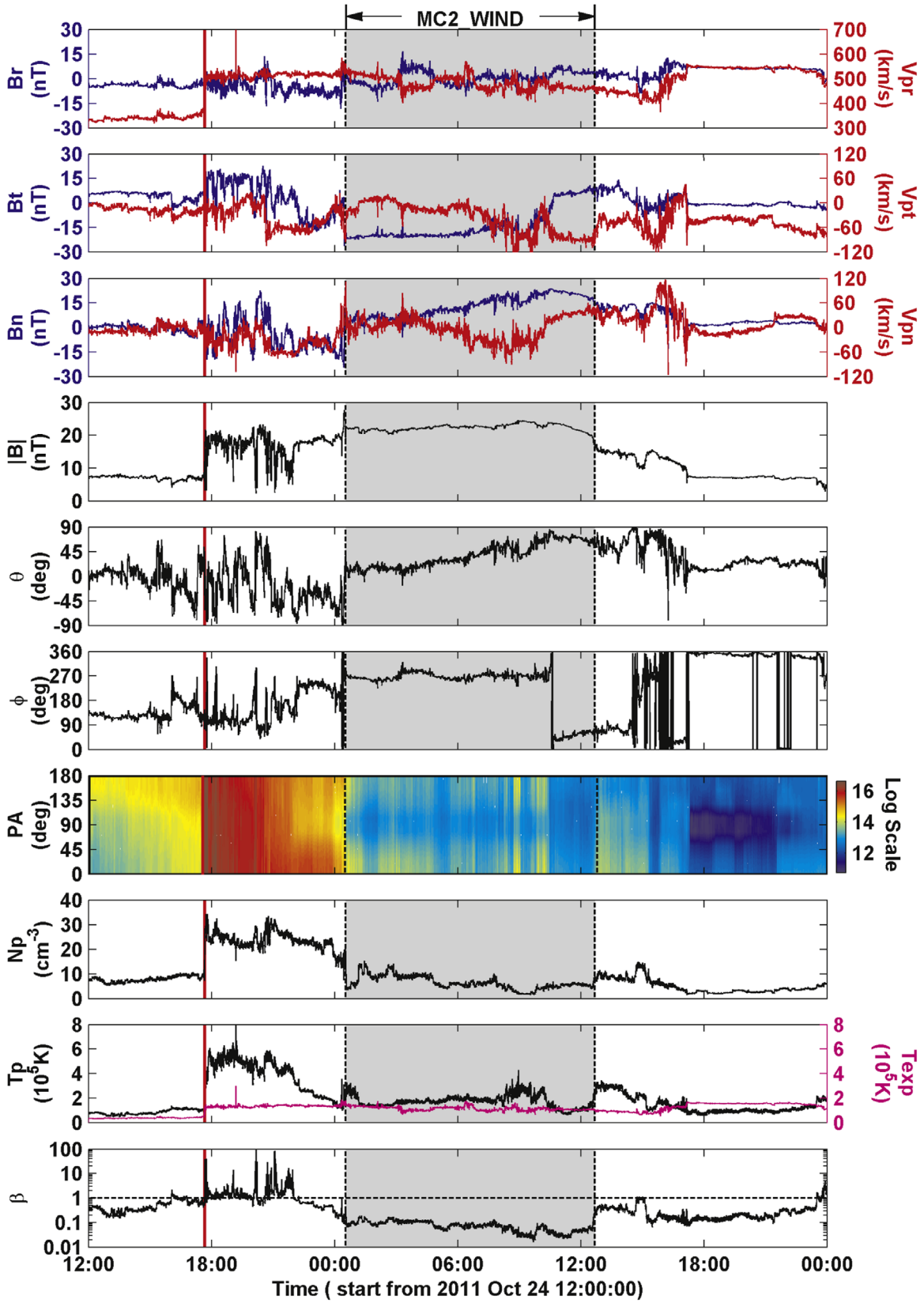

Figure 8. Same format as Figure 3 observed by *WIND* from 12:00 UT on 2011 October 24 to 00:00 UT on 2011 October 26.

to extrapolate the arrival time and speed of CME2 at *WIND* and *STA* respectively. The differences (calculated–observed) between the parameters from the Drag-based Model and the corresponding in situ parameters are given (*WIND*: −3.5 hr, −4 km s^{-1}; *STA*: −5.5 hr, 9 km s^{-1}), which means that there is a reasonable match between CME2 and in situ observers.

Excluding the confusion of CME*, MC2_WIND and MC2_STA are considered to be the observational results of

Table 1
List of MCs with Long-duration Alfvén Waves Observed by *WIND* during 1995–2015 (Retrieved from Chi et al. 2016)

No.	MC Start (UT)	MC End (UT)	C.C.(Sign)
1	1995 Apr 3 13:00:00	1995 Apr 4 12:51:25	Negative
2	1996 May 27 14:44:15	1996 May 28 11:21:25	Negative
3	1996 Aug 7 11:42:00	1996 Aug 8 08:14:59	Positive
4	1996 Dec 24 02:53:15	1996 Dec 24 13:41:15	Negative
5	1997 Jun 8 19:14:15	1997 Jun 9 23:01:30	Positive
6	1997 Oct 10 21:37:58	1997 Oct 11 14:33:11	Negative
7	1997 Nov 22 18:51:25	1997 Nov 23 12:49:30	Positive
8	1998 Jan 7 02:53:15	1998 Jan 8 07:27:45	Positive
9	1998 Mar 4 14:37:30	1998 Mar 5 20:29:09	Negative
10	1999 Aug 9 10:18:56	1999 Aug 10 16:15:00	Negative
11	2000 Oct 13 17:42:22	2000 Oct 14 15:30:05	Positive
12	2001 Apr 4 21:00:00	2001 Apr 5 09:03:23	Negative
13	2002 May 19 03:20:15	2002 May 20 04:25:30	Negative
14	2005 Dec 31 13:48:00	2006 Jan 1 15:43:52	Positive
15	2006 Apr 13 15:45:00	2006 Apr 14 11:01:29	Positive
16	2009 Feb 4 00:18:00	2009 Feb 4 16:43:30	Negative
17	2011 May 28 05:33:00	2011 May 28 21:54:00	Positive
18	2011 Sep 17 15:37:30	2011 Sep 18 08:15:00	Negative
19	2011 Oct 25 00:32:37	2011 Oct 25 12:41:37	Negative
20	2012 Feb 27 18:04:30	2012 Feb 28 14:26:15	Negative
21	2013 May 16 15:00:00	2013 May 16 22:34:30	Negative
22	2013 Oct 2 23:44:09	2013 Oct 3 14:53:26	Negative
23	2013 Nov 11 17:42:00	2013 Nov 12 01:52:30	Positive

the same magnetic rope, which both have high similarities of flux rope topology: (1) low density, low proton temperature, and low plasma β, (2) bidirectional suprathermal electron strahls, (3) unchanging of azimuthal angle in leading and middle parts, but changing sharply by 120° in the rear, and (4) elevation angle from small to large, $0° \sim 90°$ and $-45° \sim 45°$. As shown in Figure 11, the slopes of the linear regression fitting are 0.73 (0.77), 0.76 (0.74), and 0.88 (0.63) for MC2_WIND (MC2_STA). It is clearly noticeable that the correlation coefficients in MC2_WIND (MC2_STA) are found to be less than -0.7 (larger than 0.7), indicating that the fluctuations within MC2_WIND (MC2_STA) are primarily magnetic-field-direction (anti-magnetic-field-direction) Alfvén waves. To sum up, the bidirectional Alfvén waves coexist in the MC2.

4. Discussion and Conclusion

In this Letter, we enumerated two halo CMEs by using coronagraphs on board twin *STEREO* spacecraft and *SOHO* spacecraft. By analysis of two corresponding MCs observed by both *STA* and *WIND* spacecraft, it is found that there are constantly unidirectional Alfvén waves embedded within the whole MC and bidirectional Alfvén waves coexisting in a magnetic flux rope. Previous reports about Alfvén waves within MC were relatively rare. According to our comprehensive statistical analysis, only 23 (totally 163) MC events with long-duration Alfvén waves were confirmed during 1995–2015 in observation of *WIND* (as shown in Table 1, the last column lists the sign of correlation coefficients). In ambient solar wind, we always focus on whether the direction of Alfvén waves is sunward or antisunward relying on the B_r component (i.e., pointing on the Sun–spacecraft line) and the sign of correlation coefficients (Belcher & Davis 1971; Wu et al. 2017). However, a flux rope is a coherent magnetic structure in a plasma

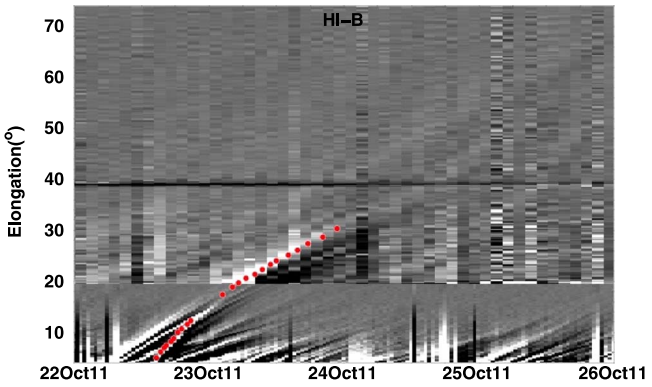

Figure 9. Time elongation (J-map) during 2011 October 22–26. The red dots indicate the track of the CME's leading edge viewed by *STB*.

consisting of helical field lines of varying pitch wrapped about a central axis, which roots at both ends in the Sun. So coherent Alfvén waves within MC should start from one footpoint, propagate along the interplanetary magnetic flux rope, and come back to the other footpoint.

The CME cross section may be close to a circle or an ellipse (Riley & Crooker 2004; Owens et al. 2006). Figure 12 illustrates the schema of two large-scale MCs (MC1 and MC2) launched from the Sun. For MC1, a shock was driven before the main body of the flux rope (black dashed lines represent the propagating direction of main body), which was identified by *STA* but not by *WIND* spacecraft. Thus we infer that MC1 encountered *STA* with its main body and sweeped *WIND* spacecraft with its flank. In the observations of both spacecraft, the coherent unidirectional Alfvén waves are embedded within the whole MC1 propagating in the reverse direction of MC1's axis. Next, MC2 is the first reported observation of bidirectional Alfvén waves within a magnetic flux rope in the solar wind, like two sets of Alfvén waves, respectively, launching from two roots.

As shown in Figures 3 and 4, Alfvénic fluctuations with correlated changes in magnetic field and velocity were also present both upstream and downstream of the MC1. We notice that the fluctuations upstream and downstream exhibited features obviously different from those within MC1, involving (1) positive correlation for MC1, but negative correlation for upstream and downstream, (2) larger timescales of the magnetic field and velocity variations within MC1, and (3) lower amplitudes of the magnetic field and velocity variations within MC1. Such dissimilar properties imply quite different forms and entirely disparate sources. Subsequently, we apply a trial of the MVA method to extract the information of magnetic oscillation (i.e., azimuthal perturbations). Figure 13 shows the hodograph of the $B_l - B_m$ magnetic field components (the plane perpendicular to the minimum eigenvector direction) for three 10 minute intervals in MC1_WIND and MC1_STA. It is clearly visible that the magnetic field within the whole MC1 undergoes irregular alternate rotations along an arc through a relatively small angle, which is consistent with the clue of a torsional Alfvén wave within a flux rope (Guo et al. 2019). Nevertheless, the fluctuations upstream and downstream behave like an arc through a large angle in the hodograph, which is well interpreted as arc-polarized Alfvén waves in the solar wind (see Wang et al. 2012, Figure 5). Meanwhile, we

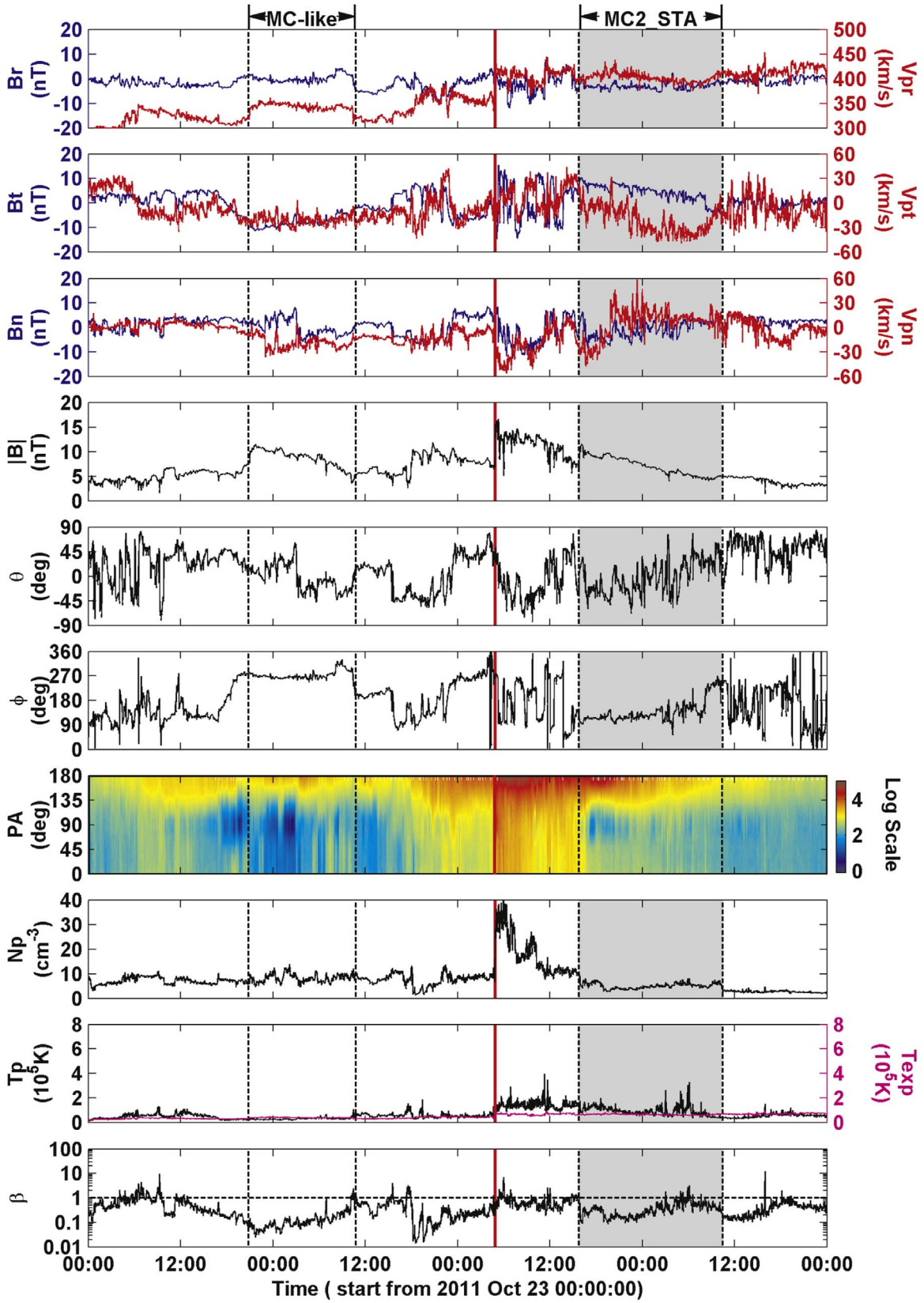

Figure 10. Same format as Figure 4 observed by *STA* during 2011 October 23–27.

extract no similar torsional information from the bidirectional Alfvén waves within MC2. The different CME triggering models are more or less associated with magnetic reconnection or shearing motion of magnetic field lines (Liang et al. 2012). For example, in the CSHKP model (Carmichael 1964; Sturrock 1966; Hirayama 1974; Kopp & Pneuman 1976), abundant Alfvén waves could be immersed in the outflow region of the magnetic reconnection during the CME initiation process. In

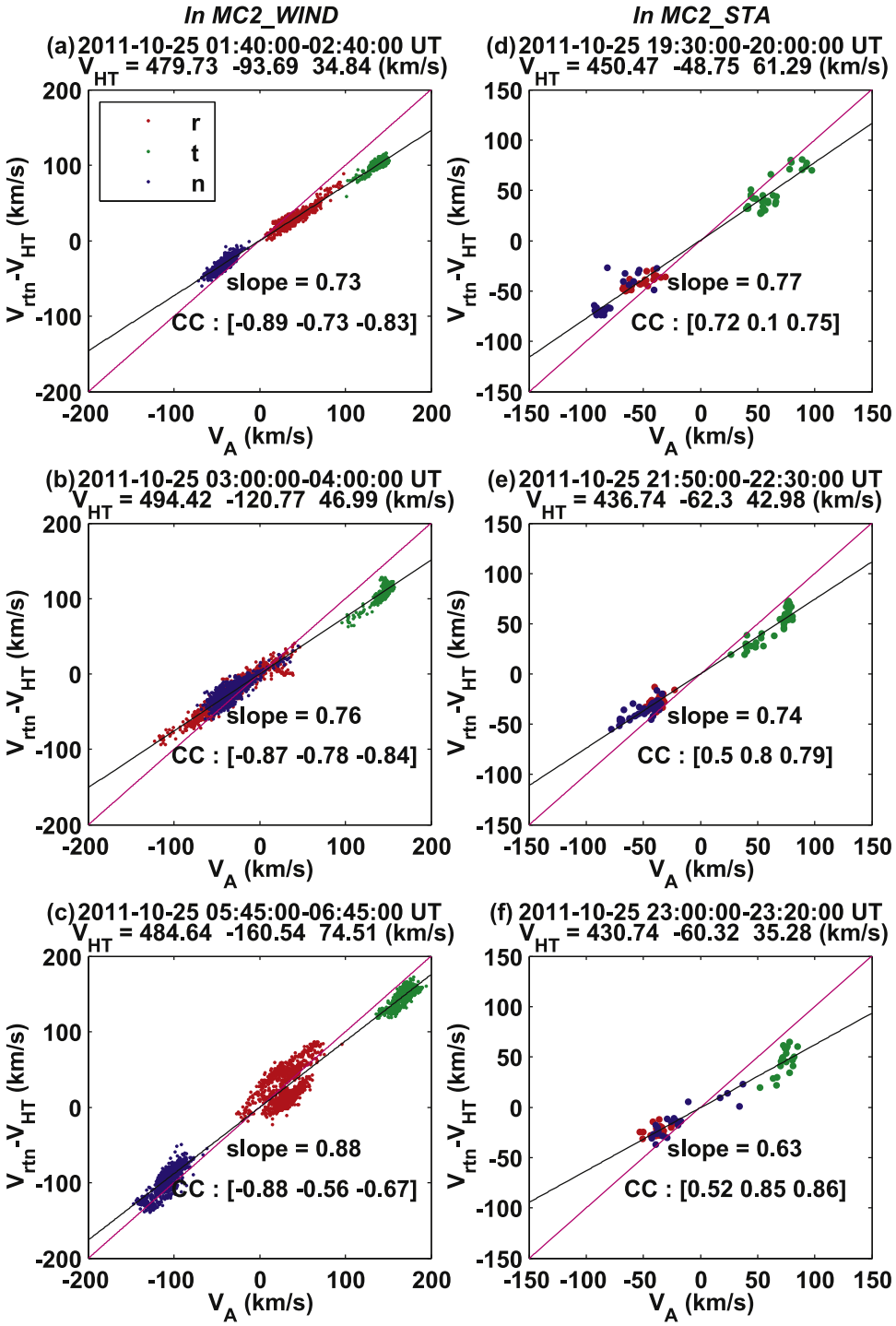

Figure 11. Same format as Figure 5 for different segments of MC2_WIND and MC2_STA.

the magnetic breakout model (Antiochos et al. 1999), the collapse of the horizontal current sheet might generate Alfvén waves confined to a narrow surface layer of the flux rope. Hence, it is reasonably speculated that there are two possible sources of Alfvén waves within flux ropes in the solar wind. The coherent unidirectional Alfvén waves, with a torsional clue, might be generated by distortions produced within a preexisting flux rope, which is consistent with the report of Gosling et al. (2010). The bidirectional arc-polarized Alfvén waves within one flux rope might be emitted from the center of reconnection during the eruption of CME, then travel outward along with two loop legs of the flux rope (no torque produced by reconnection leads to no torsional information).

In addition, it is clearly visible that MC1 encountered *WIND* spacecraft ∼13 hr earlier than *STA* (MC1's flank arrived before the main body). Wang et al. (2014) presented the time difference of CME arrival as caused by its circular-like front, and specifically CME's main body arrives before its flank. However, the kinematic process of CME in interplanetary space is complex. Shen et al. (2012) observed a comprehensive image of a super-elastic collision between two successive CMEs in the heliosphere. Burlaga et al. (2003) also found

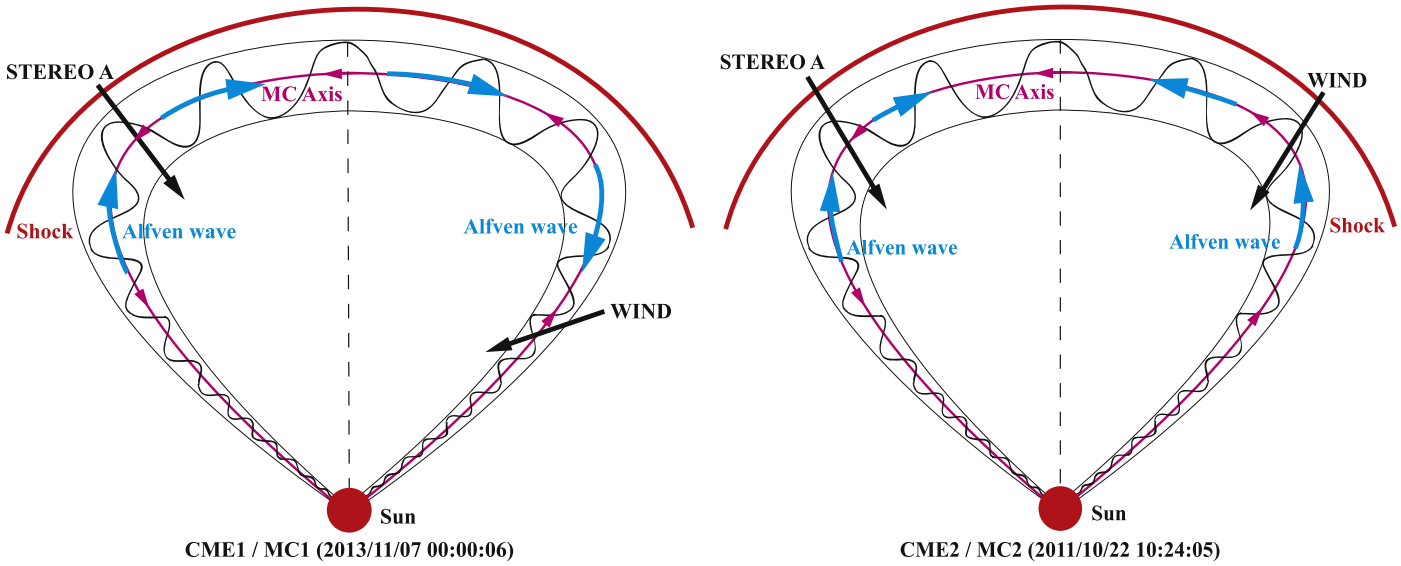

Figure 12. Schema showing two large-scale MCs launched from the Sun. Idealized global geometry of magnetic flux rope with pink arrows indicating the orientation of MC axis and the blue arrows indicating the propagating direction of Alfvén waves within MC. The two black arrows show the trajectories of *STA* and *WIND*. CME1 and CME2 were twisted in a left-hand sense and a right-hand sense, respectively.

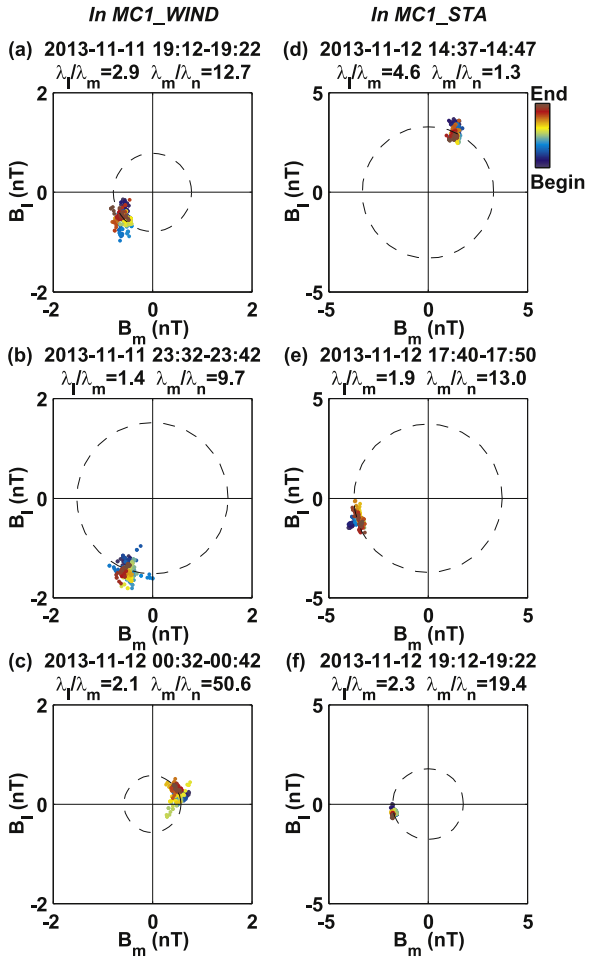

Figure 13. Hodogram of the magnetic field B_l and B_m components (along the maximum and intermediate variance directions respectively) in the plane perpendicular to n direction (the minimum variance direction) during 10 minute intervals within MC1_WIND (left) and MC1_STA (right). The ratio of the maximum to the intermediate eigenvalue (λ_l/λ_m) and that of the intermediate to the minimum eigenvalue (λ_m/λ_n) are shown.

evidence for the interaction between MCs and corotating interaction regions within 1 au. Furthermore, the CME direction of propagation could be deflected by solar wind (Wang et al. 2014), and the different ambient solar wind conditions can cause the distortion of the shape of CME (Owens et al. 2017; Scott et al. 2019). For the giant CME, the interplanetary environment differs greatly in different propagating directions, thus it might cause the magnetic rope topology to deviate from the regular appearance as it travels far away from the Sun. The shape of the front boundary of a large-scale MC might be more complicated than previously thought.

The authors would like to thank the referee for providing helpful suggestions that improved our manuscript. The data for this work are available at the official websites of *STEREO*, *SOHO*, and *WIND* spacecraft. We acknowledge the use of them. The work is jointly supported by the National Natural Science Foundation of China (grant Nos. 41731067, 41531073, 41874202, and 41861164026), the Collaborating Research Program of CAS Key Laboratory of Solar Activity, and the Specialized Research Fund for State Key Laboratories.

ORCID iDs

Zehao Wang https://orcid.org/0000-0002-2008-5510
Xueshang Feng https://orcid.org/0000-0001-8605-2159

References

Acuña, M. H., Curtis, D., Scheifele, J. L., et al. 2008, SSRv, 136, 203
Antiochos, S. K., DeVore, C. R., & Klimchuk, J. A. 1999, ApJ, 510, 485
Barnes, A., & Hollweg, J. V. 1974, JGR, 79, 2302
Belcher, J. W., & Davis, L., Jr. 1971, JGR, 76, 353
Brueckner, G. E., Howard, R. A., Koomen, M. J., et al. 1995, SoPh, 162, 357
Burlaga, L., Berdichevsky, D., Gopalswamy, N., Lepping, R., & Zurbuchen, T. 2003, JGRA, 108, 1425
Burlaga, L., Sittler, E., Mariani, F., & Schwenn, R. 1981, JGR, 86, 6673
Carmichael, H. 1964, NASSP, 50, 451
Chi, Y., Shen, C., Wang, Y., et al. 2016, SoPh, 291, 2419
Copil, P., Voitenko, Y., & Goossens, M. 2008, A&A, 478, 921
Davies, J. A., Harrison, R. A., Rouillard, A. P., et al. 2009, GeoRL, 36, L02102

Denskat, K. U., & Burlaga, L. F. 1977, JGR, 82, 2693
Doorsselaere, T. V., Nakariakov, V. M., & Verwichte, E. 2008, ApJL, 676, L73
Fan, Y. 2009, ApJ, 597, 1529
Galvin, A. B., Kistler, L. M., Popecki, M. A., et al. 2008, SSRv, 136, 437
Gopalswamy, N., Lara, A., Yashiro, S., Kaiser, M. L., & Howard, R. A. 2001, JGR, 106, 29207
Gosling, J. T. 1990 (Physics of Magnetic Flux Ropes, Geophysics Monograph Vol. 58) ed. C. T. Russell, E. R. Priest, & L. C. Lee (Washington, DC: American Geophysical Union), 343
Gosling, J. T., Teh, W. L., & Eriksson, S. 2010, ApJL, 719, L36
Guo, J., Wang, Z. H., Feng, X., et al. 2019, ApJL, 874, L19
He, J., Zhu, X., Chen, Y., et al. 2018, ApJ, 856, 148
Hirayama, T. 1974, SoPh, 34, 323
Howard, R. A., Moses, J. D., Vourlidas, A., et al. 2008, SSRv, 136, 67
Jang, S., Moon, Y. J., Kim, R. S., Lee, H., & Cho, K. 2016, ApJ, 821, 95
Jess, D., Mathioudakis, M., Erdselyi, R., et al. 2009, Sci, 323, 1582
Kopp, R. A., & Pneuman, G. W. 1976, SoPh, 50, 85
Lepping, R. P., Acuña, M. H., Burlaga, L. F., et al. 1995, SSRv, 71, 207
Li, H., Wang, C., He, J., et al. 2016, ApJL, 831, L13
Liang, H. M., Xiao, C. J., Zhou, G. P., et al. 2012, PlST, 14, 2
Lin, R. P., Anderson, K. A., Ashford, S., et al. 1995, SSRv, 71, 125
Liu, Y., Richardson, J. D., Belcher, J. W., Kasper, J. C., & Elliott, H. A. 2006, JGRA, 111, A01102
Longcope, D. W., & Welsch, B. T. 2000, ApJ, 545, 1089
Marsch, E., Yao, S., & Tu, C. Y. 2009, AnGeo, 27, 869
Möstl, C., Amla, K., Hall, J. R., et al. 2014, ApJ, 787, 119
Owens, M. J., Lockwood, M., & Barnard, L. A. 2017, Sci, 7, 4152
Owens, M. J., Merkin, V. G., & Riley, P. 2006, JGRA, 111, A03104
Raghav, A. N., & Kule, A. 2018, MNRASL, 476, L6
Riley, P., & Crooker, N. U. 2004, ApJ, 600, 1035
Sauvaud, J. A., Larson, D., Aoustin, C., et al. 2008, SSRv, 136, 227
Scott, C. J., Owens, M. J., de Koning, C. A., et al. 2019, SpWea, 17, 539
Shelyag, S., Cally, P. S., Reid, A., & Mathioudakis, M. 2013, ApJL, 776, L4
Shen, C., Wang, Y., Pan, Z., et al. 2014, JGRA, 119, 5107
Shen, C., Wang, Y., Wang, S., et al. 2012, NatPh, 8, 923
Shi, T., Wang, Y. K., Wan, L. F., et al. 2015, ApJ, 806, 271
Sonnerup, B. U. O., Papamastorakis, I., Paschmann, G., & Luhr, H. 1987, JGR, 92, 12137
Sturrock, P. A. 1966, Natur, 211, 695
Tian, H., Yao, S., Zong, Q., et al. 2010, ApJ, 720, 454
Vasheghani, F. S., Nakariakov, V. M., Van, D. T., & Verwichte, E. 2011, A&A, 526, A80
Wang, X., He, J., Tu, C., et al. 2012, ApJ, 746, 147
Wang, Y., Wang, B., Shen, C., Shen, F., & Lugaz, N. 2014, JGRA, 119, 5117
Wu, H., Wang, X., Tu, C., et al. 2017, JGRA, 122, 9768
Yao, S., Marsch, E., Tu, C., & Schwenn, R. 2010, JGRA, 115, A05103